Eur. Phys. J. D **19**, 183–192 (2002)
DOI: 10.1140/epjd/e20020070

THE EUROPEAN PHYSICAL JOURNAL D
EDP Sciences

Fragmentation and reliable size distributions of large ammonia and water clusters

C. Bobbert[a], S. Schütte[b], C. Steinbach, and U. Buck[c]

Max–Planck–Institut für Strömungsforschung, Bunsenstraße 10, 37073 Göttingen, Germany

Received 21 November 2001

Abstract. The interaction of large ammonia and water clusters in the size range from $\langle n \rangle = 10$ to 3 400 with electrons is investigated in a reflectron time-of-flight mass spectrometer. The clusters are generated in adiabatic expansions through conical nozzles and are nearly fragmentation free detected by single photon ionization after they have been doped by one sodium atom. For ammonia also the (1+1) resonance enhanced two photon ionization through the $\tilde{A}$ state with $v = 6$ operates similarly. In this way reliable size distributions of the neutral clusters are obtained which are analyzed in terms of a modified scaling law of the Hagena type [Surf. Sci. **106**, 101 (1981)]. In contrast, using electron impact ionization, the clusters are strongly fragmented when varying the electron energy between 150 and 1 500 eV. The number of evaporated molecules depends on the cluster size and the energy dependence follows that of the stopping power of the solid material. Therefore we attribute the operating mechanism to that which is also responsible for the electronic sputtering of solid matter. The yields, however, are orders of magnitude larger for clusters than for the solid. This result is a consequence of the finite dimensions of the clusters which cannot accommodate the released energy.

PACS. 36.40.-c Atomic and molecular clusters – 36.40.Qv Stability and fragmentation of clusters – 61.46.+w Nanoscale materials: clusters, nanoparticles, nanotubes, and nanocrystals

1 Introduction

Clusters play an increasing and important role in many areas of physics and chemistry [1]. While the production of all types of clusters in all size ranges provides nowadays no problems, their detection and a reliable determination of their size distributions is still not trivial. The reason is the ubiquitous fragmentation which usually occurs when the clusters are ionized [2]. This is a special problem for weakly bound systems, since the ionic potential curves are usually much stronger bound and shifted to smaller equilibrium values compared to their neutral precursors, so that, because of the unfavorable Franck-Condon factors, the system reaches when going from the neutral to the ionized configuration a highly excited vibrational state [2,3]. The available excess energy then leads to the evaporation of atoms or molecules so that even at the threshold without external excess energy fragmentation occurs. This pure molecular mechanism is also operating in larger clusters, since the charge usually localizes at a special ion (X_3^+ and X_4^+ for rare gases [4]) which is then surrounded by neutral species that can evaporate. For molecular systems the originally formed ions might react with its neighbors [5] and, for hydrogen bonded systems, often protonated ions are observed. This was indeed measured for small clusters of ammonia and water, the two systems studied in this contribution. For size selected clusters [6], appreciable fragmentation was observed with fragment ions centered around NH_4^+ [7] and D_3O^+ [8]. This mechanism is considered to operate mainly for small clusters and should become less and less important for larger clusters, since the increasing number of degrees of freedom can easier accommodate the available energy [9,10].

Recently, however, we observed that also large clusters exhibit strong fragmentation for electron impact if the energies are increased up to 1 500 eV. Originally, this effect was at first observed for large ammonia clusters where it also occurred for high intensity laser pulses. A preliminary account with emphasis on the photoionization was published in the proceedings of a meeting [11]. In order to find the origin for this behavior, we extended the measurements to another hydrogen bonded system, to water clusters, and to the heavier rare gas clusters that are typical van der Waals systems [12]. They all exhibit the same effects which are even more pronounced for the rare gases where 8 560 atoms evaporated from a Xe_n cluster of $\langle n \rangle = 10\,280$. We attribute this effect to a behavior that is well-known from the electronic sputtering of solid insulator matter [13,14]. Here the photon, electron or fast ion

[a] *Present address*: Heinrich Hertz Institut, 10587 Berlin, Germany.
[b] *Present address*: Agilent Technologies, 76337 Waldbronn, Germany.
[c] e-mail: ubuck@gwdg.de

that impinges on the solid deposits its energy in electronic excitations of the atoms or molecules of the solid. When this energy is rapidly dispersed in these insulators, it may be coupled to the atomic motions and then transported to the surface where on the average about 2 to 20 atoms or molecules escape per incoming particle. For clusters these numbers are found to be much higher which is a consequence of their finite size. We note that we only consider the interaction of one electron with the cluster.

In this paper we will present extended data sets for both ammonia and water clusters and will discuss the implications of the applied model. A crucial condition for the experiments is the determination of a reliable size distribution without fragmentation. This is obtained by doping them with one sodium atom. Both systems are known to form weakly bound systems with alkali atoms whose ionization potential is appreciably reduced compared to that of pure sodium [15]. Thus it is easy to photoionize them with one photon directly at the threshold. For ammonia we found with the (1+1) resonance enhanced multi photon ionization (REMPI) through the $\tilde{A}$ state a very interesting complementary way for a soft ionization that is usually not available for such molecular systems. In addition, we have analyzed the size distribution for ammonia and water and have tried to derive reliable scaling laws for these systems which are only known for atomic species [16,17]. Moreover, we observed in a special range of source conditions and particularly pronounced for water clusters, a bimodal size distribution that we attribute to a transition in the cluster production.

The paper is organized as follows. We will briefly describe the experimental arrangement which consists of a cluster source, a doping device for Na, a pulsed electron beam and the different laser sources for ionization, and finally, the reflectron time-of-flight mass spectrometer for detection. Then the results for the size distributions and the fragmentation pattern are presented and discussed.

2 Experimental

The experiments have been carried out in a molecular beam machine which has been described in detail in reference [12]. Therefore we will present here only a short account of the main parts with emphasis on those that have been changed. The machine consists of a source chamber, a buffer chamber and a detector unit. The clusters are produced by adiabatic expansion through a nozzle of conical shape. Both pulsed and continuous beams have been generated. The ammonia clusters are generated by expansion through a conical nozzle with the diameters 64, 76, and 350 μm, the opening angles 24.4°, 20.1°, and 28.6°, and the lengths 2, 6, and 7.7 mm, respectively. The pressure varied between 0.5 and 8.0 bar at temperatures of 308 to 503 K. The pulsed nozzle is piezo driven and follows a construction proposed in the literature [18]. The water clusters are produced as continuous beams by expanding water vapor between 1.5 and 21 bar through a nozzle of conical shape with diameters between 50 and 138 μm, opening angles between 24.4° and 41°, and lengths of 2 and 4 mm.

The clusters are detected in a reflectron time-of-flight mass spectrometer. The design of the ion source allows us to simultaneously use laser photons and electrons for ionization. The electron pulses are produced by the impact of the photon pulse on two copper electrodes. This is an improved version of a previously published arrangement [19]. The details are given in reference [20]. By applying suitable pulsed voltages at the two copper electrodes, we obtain a reliable electron source with variable energy in the range from 50 eV to 1 500 eV, a pulse width of about 12 ns and currents between 10 and 300 mA. Under optimal conditions, a mass resolution of $m/\Delta m = 1\,600$ was obtained at $m = 200$ u, based on the drift length of 1 820 mm. The current density of this electron beam is still small enough to rule out any multi-electron processes even for the largest clusters investigated here.

The ions are extracted in the direction of the beam and detected on a microsphere plate. The mass spectra are detected using a digital storage oscilloscope in a special particle counting mode. The spectra are corrected for the size dependence of the detection probability and the ionization cross-section, the transformation from time to mass coordinates, and double ionization processes.

In order to get reliable size distributions that are only weakly perturbed by fragmentation we have to apply an ionization method close to the threshold with potential curves which do not differ very much for the neutral and the ionic system so that low lying vibrational states can be reached. The doping of the ammonia and water clusters with one sodium atom is an ideal tool for this purpose. The presence of the sodium atom leads to largely delocalized electron distributions with the consequence that the potential curves for the neutral and the ionic systems are very similar [21–23]. In addition, the ionization potential is largely reduced from 5.1 eV for the bare atom to 3.2 eV for larger water clusters [15] and to values between 3.6 eV and 2.1 eV for ammonia clusters between $n = 2$ to $n = 100$ [15,24]. These values can be easily reached by dye lasers and are, additionally, far below the ionization potentials of the bare molecules. In half of the experiments we generated these doped clusters by crossing the bare cluster beam with a low pressure sodium beam close to the expansion as is described in detail in reference [12]. In the other half of the experiments the molecular clusters were doped by passing through a scattering cell which was built in the buffer chamber. In this way much lower pressures could be used and the original expansion was not at all perturbed.

Originally, the ammonia clusters were ionized by resonance enhanced two photon ionization (REMPI). This is by no means a straightforward procedure, since these processes that work so well for molecules usually fail to work for clusters because of the enhanced possibilities for a rapid decay of the excited state. Following the literature we first applied the (1+1)-REMPI process *via* the $\tilde{A}\ ^1A_2''$ $v = 2$ state at 208 nm. It worked successfully up to $n = 7$ by shifting a little bit the resonance frequency to

Table 1. Source conditions, reduced scaling parameter $\Gamma^\star$ derived from the value q given in Table 3, and measured mean clustersize $\langle n \rangle$ for ammonia clusters. The reservoir temperature is 308 K in all cases.

d/μm	$2\alpha/^\circ$	l/mm	p_0/bar	T_0/K	$\Gamma^\star$	$\langle n \rangle$
76	20.1	6.0	1.05	308	2 499	80
			1.5	308	3 571	170
			2.0	308	4 758	346
			2.5	308	5 946	461
			3.0	308	7 140	579
			3.5	308	8 329	655
			4.0	308	9 514	706
			4.0	353	6 913	653
			4.0	403	5 069	278
			4.0	433	4 284	196
			4.0	463	3 662	116
			4.0	503	3 017	83
350	28.6	7.7	1.0	312	4 968	272
			1.5	312	7 456	829
			2.0	312	9 935	1 182
			3.0	312	14 910	1 537
			4.0	312	19 867	1 634
			5.0	312	24 855	2 089
			6.0	312	29 816	2 555
			7.0	312	34 780	3 028
			8.0	312	39 767	3 391

Table 2. Source conditions, reduced scaling parameter $\Gamma^\star$ derived from the value q given in Table 3, and measured mean clustersize $\langle n \rangle$ for water clusters.

d/μm	$2\alpha/^\circ$	l/mm	T_s/K	p_0/bar	T_0/K	$\Gamma^\star$	$\langle n \rangle$
50	41.0	2	386	1.577	495	1 084	9
			396	2.173	495	1 455	20
			406	2.942	495	1 922	35
			416	3.919	495	2 497	54
			426	5.144	495	3 204	80
			437	6.827	495	4 142	130
			445	8.307	495	4 949	338
			456	10.745	495	6 248	587
			467	13.714	495	8 103	765
			479	17.647	544	7 814	649
			479	17.647	573	6 909	498
			479	17.647	608	6 004	458
			479	17.647	651	5 108	360
			479	17.647	694	4 390	219
79	25.0	4	412	3.5	493	4 232	154
			432	6.0	493	6 922	704
			446	8.5	493	9 494	1 010
			453	10.0	508	10 244	1 177
			465	13.0	496	13 725	1 301
			471	15.0	498	15 483	1 262
			480	18.0	505	17 652	1 750

210.5 nm [25]. We have extended this result up to $n = 15$ using laser pulses in the nanosecond regime. Later on it was shown using femtosecond pump-probe analysis for this state that the decay times are in the order of 250 to 900 fs so that the failure to detect larger clusters could be explained. Using these femtosecond laser pulses cluster sizes up to $n = 100$ were detected [26]. We were successful in detecting ammonia clusters up to several thousand molecules using the same $\tilde{A}\ ^1A_2''$ state but the higher vibrational state $v = 6$ at 193 nm [27]. Apparently the lifetime of this state in the cluster environment is long enough to be reached by the second photon in the nanosecond regime. A possible candidate for such long-lived states is the intermediate component $NH_4(NH_3)_n$ for which for $n \geq 3$ lifetimes longer than 10 μs have been observed [28,29]. In this experimental arrangement we can produce and detect ammonia clusters in the size range from $n = 10$ to 3 000. The results will be presented in Section 3. For an application of these clusters in a scattering experiment we refer to reference [30].

3 Results and discussion

3.1 Size distributions

The basis of the reliable determination of the fragmentation is an accurate measurement of the unperturbed cluster size distribution. For ammonia two methods are available. In the first one the clusters are doped by one sodium atom and then photoionized using a dye laser at $\lambda = 395$ nm (3.15 eV). This is exactly at the threshold of the trimer. For larger clusters in the range of $n = 100$ with ionization potentials around 2.0 eV about 7 to 10 additional molecules might be evaporated. We have measured more than 80 mass spectra for different source conditions. We will here only present a selection that exhibits the characteristic features. These data are shown for ammonia in Table 1 and water in Table 2. Further data are available from the authors by request. The results for the mass spectra of ammonia clusters using a conical nozzle with a diameter of 76 μm, an opening angle of $2\alpha = 20.1^\circ$, and a length of $l = 6$ mm are depicted in Figure 1 for different source pressures p_0 and nozzle temperatures T_0. The second method is the (1+1)REMPI photoionization at $\lambda = 193$ nm (12.8 eV) of the bare molecular cluster. Here multi-photon processes have to be taken into account, which lead to fragmentation with a linear dependence of the power density, *i.e.* number of absorbed photons. The mass spectra can be corrected for this fragmentation by extrapolating to a power density of zero. For the bare (1+1)REMPI process assuming an estimated ionization potential of IP = 8.6 eV and bonding energies of about 200 meV the number of evaporated molecules is smaller than 25 even if we take into account an additional energy release from internally vibrational excited molecular ions originating from fast inter-cluster reactions. The comparison of the mass spectra taken under the same source conditions using the two different methods shows, within the usual day to day fluctuations of the cluster beam source of about 10%, good agreement. Using a pulsed conical nozzle with a diameter of 350 μm, an opening angle of $2\alpha = 28.6^\circ$, and a length of 7.7 mm much larger cluster sizes

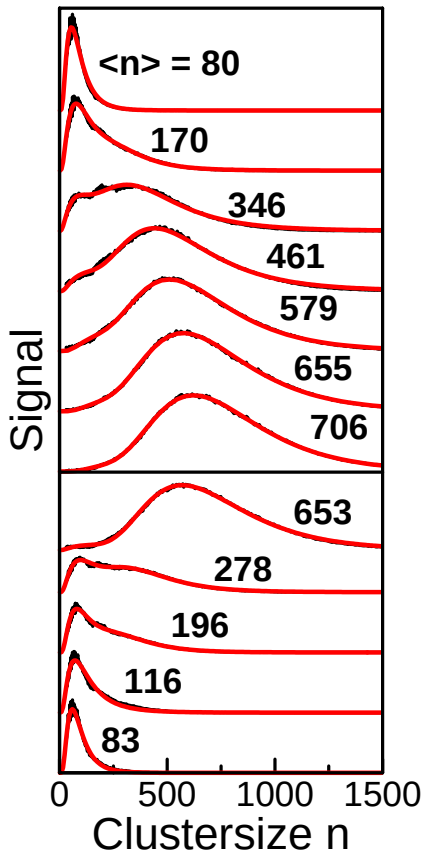

Fig. 1. Measured mass spectra of ammonia clusters doped by Na atoms and detected by single photon ionization for different source pressures (upper part) and different temperatures (lower part). The average sizes $\langle n \rangle$ indicated are determined from the fitted log-normal distributions specified by the solid lines. For the source conditions see Table 1, first block.

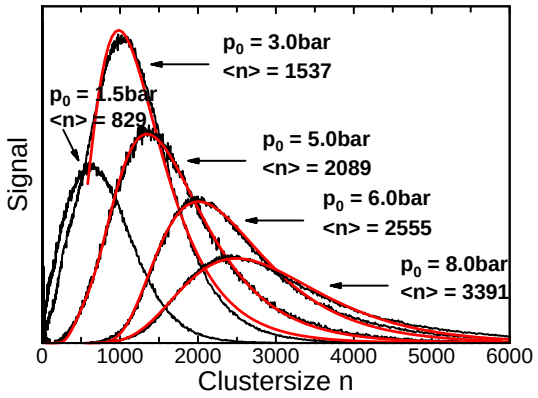

Fig. 2. Measured mass spectra of ammonia clusters detected by (1+1) REMPI photoionization for different pressures. The average sizes indicated are determined from the fitted log-normal distributions specified by the solid lines. For the source conditions see Table 1, second block. The average cluster sizes presented here and in Table 1 are corrected for fragmentation caused by the multi-photon processes.

were generated as is illustrated in Figure 2. The values for the average size $\langle n \rangle$ given in Table 1 are corrected for the fragmentation caused by multi-photon processes according to the applied power density of the laser. This effect was measured in reference [11]. Depending on the source conditions the shape of the size distribution goes over from the typical exponential decay at small average sizes to the log-normal distribution at large average sizes. While in the former case the production process is dominated by monomer addition, the latter shape results from the coagulation of larger entities. The solid lines in the figures are fits to the experimental data using

$$f(n) = \frac{1}{\sqrt{2\pi}\sigma n} \exp\left[-\frac{(\ln n - \mu)^2}{2\sigma^2}\right] \qquad (1)$$

with the two parameters μ, the logarithm of the geometric mean, and σ, the logarithm of the geometric standard deviation. The mean cluster sizes that are also given in the figures are directly determined from the fit. In case of the exponential type curves, they are calculated from the integrated spectra by setting $\int_0^{\langle n \rangle} f(n)\mathrm{d}n = 0.5$. Such a behavior has been observed many times before [31], but what is new is that we definitely measure a transition between two type of shapes in the region of $\langle n \rangle = 350$ where a bimodal distribution results. Both peaks can be fitted by log-normal distributions. With increasing pressure or decreasing temperature, apparently the first peak disappears at the expense of the second one. We also note that the description of the distribution by a log-normal shape is an extremely well representation especially for large cluster sizes.

In the case of water clusters only the doping method was employed using photons of $\lambda = 360$ nm (3.46 eV). Here we are close to the threshold of all doped $Na(H_2O)_n$ clusters for $n \geq 4$ so that a nearly fragmention free ionization results. The measured water mass spectra using a conical nozzle with a diameter of 50 μm, an opening angle of $2\alpha = 41°$, and a length of 2 mm are depicted in Figure 3. The middle part exhibits the pressure dependence, the lower part the temperature dependence, and the upper part the pressure dependence at a different nozzle diameter. Here a conical nozzle with a diameter of 79 μm, an opening angle of $2\alpha = 25°$, and a length of 4 mm was used. In general, the expected behavior is observed. At small cluster sizes, the exponential behavior dominates and, at large cluster sizes, the measured curves can all be fitted nearly perfectly by log-normal distributions. In the intermediate range, we observe interestingly a bimodal distribution as was already mentioned for ammonia. The two peaks can both be fitted by individual log-normal distributions. It occurs when the pressure is increased at constant temperature (middle part) and when the temperature is lowered at constant pressure (lower part). The origin of this effect is obviously a different production process, since fragmentation can be ruled out as origin of this behavior. We think that the peak at lower size can be traced back to the growing of cold solid clusters by addition of small complexes, say dimers or trimers, to the cluster. In contrast, the peak at larger sizes is definitely based on the coagulation of larger pieces.

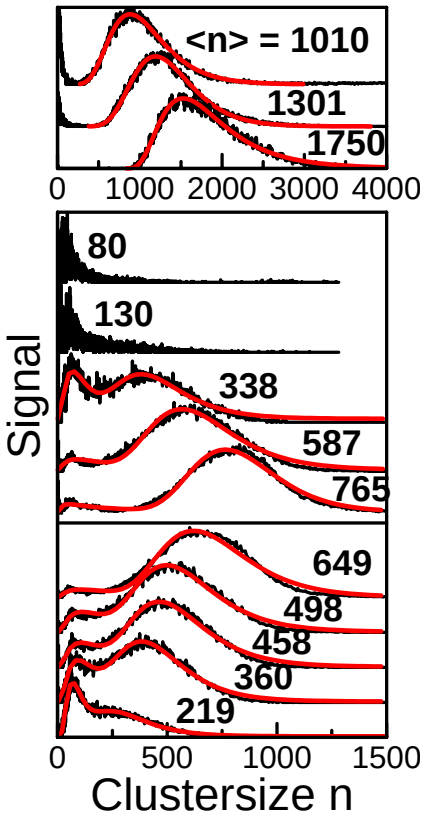

Fig. 3. Measured mass spectra of water clusters doped by Na atoms and detected by single photon ionization. Lower panel: variation of temperature; middle panel: variation of pressure; upper panel: variation of nozzle diameter and pressure. The average sizes indicated are determined from the fitted log-normal distributions specified by the solid lines. For the source conditions see Table 2, from top to bottom of the figure, second block and first block of the table.

A plausible explanation might be that because of the addition of larger parts with larger energy release the cluster is first liquid and then cools off by evaporation. The first mechanism is usually assumed to be the main process in the cluster production of small systems. The latter one has been invoked by the extensive investigation of the condensation of large water clusters by electron diffraction [32]. We note that in some cases the intensity gap between the two peaks is filled up and that, in any case, the average size fits very well into the general development of cluster sizes.

The general scaling laws that correlate the mean cluster size $\langle n\rangle$ with the source conditions were established by Hagena [16,17]. While the cluster formation is dominated by bimolecular collisions, the decay processes are governed by unimolecular reactions. The key parameter that correlates the flow which produces the same cluster size is given by

$$\Gamma = n_0 d^q T_0^{sq-f/2} (0 < q \leq 1). \quad (2)$$

Here n_0, T_0, and d are the source density, nozzle temperature and nozzle diameter, f is the number of energetically active degrees of freedom and $s = (f-2)/4$ for axial symmetric flows. The main temperature dependence originates from the isentropic expansion expressed by f. The parameter q is introduced *ad hoc* to account for the slower flow at larger nozzle diameters by an empirical relation and is usually determined experimentally. The shape of the nozzle is taken into account by the concept of equivalent nozzles that are responsible for the same flow properties [16]. A widely used class of supersonic nozzles are those of conical shape with a cone angle of 2α and a throat diameter d. In this case the equivalent nozzle diameter $d_{\rm eq}$ is given by

$$d_{\rm eq} = G(f) d/\tan\alpha;\ G(f) = 0.5(f+1)^{-(f+1)/4} A^{f/2}. \quad (3)$$

A is the constant calculated by Ashkenas and Sherman [33] that connects the Mach number $M = A(x/d)^{2/f}$ with the reduced distance x/d. For the molecular systems studied here with $f = 6$ (3 translational and 3 rotational degrees of freedom) we obtain $s = 1$ and, with $A = 3.83$ for a three-dimensional axisymmetric flow, $G(f) = 0.933$. We note that $d_{\rm eq}$ does not depend on the length of the nozzle, since the decrease of intensity as function of the distance is compensated by the increasing area. For the scaling parameter we get $\Gamma = n_0 d_{\rm eq}^q T_0^\alpha$ with $\alpha = q-3$.

This concept can be extended to different gases by applying the law of corresponding states. This is certainly valid for the monoatomic rare gases, but it also proved to be a viable idea for metals [17]. For the characteristic values to reduce the length and energy (temperature) variables the ratio mass m to density ρ and the sublimation enthalpy Δh were used

$$r_{\rm ch} = (m/\rho)^{1/3}\ ;\ kT_{\rm ch} = \Delta h. \quad (4)$$

The values for ammonia are $r_{\rm ch} = 3.20$ Å and $T_{\rm ch} = 3\,510$ K. For water we employ $r_{\rm ch} = 3.19$ Å and $T_{\rm ch} = 5\,684$ K. Based on $K_{\rm ch} = r_{\rm ch}^{q-3} T_{\rm ch}^\alpha$ the reduced scaling parameter

$$\Gamma^* = \Gamma / K_{\rm ch} \quad (5)$$

is introduced. If this is also a good approximation for molecular clusters where the interaction potentials are anisotropic has to be checked against experimental results. Finally, the mean clustersize $\langle n\rangle$ is given according to Hagena by a simple power law

$$\langle n\rangle = D \left(\frac{\Gamma^*}{1\,000}\right)^a. \quad (6)$$

Thus in a log-log-plot a linear behaviour should result. We fitted the experimental data by the optimization of the free parameters q, D and a. The results are depicted in Figure 4 and listed in Table 3. The exponent of the temperature dependence is calculated from the relation $q-3$ and also given in Table 3. In both cases the expected linear relationship is obtained. The value of q is smaller than that estimated for the rare gases (0.85), but is still in the range that could be expected. To check the accuracy of the temperature dependence of this law, we carried

Table 3. Optimized values q, α, D and a for scaling the size of ammonia and water clusters. The numbers in parenthesis give the error of the corresponding digits.

	q	$q-3$	α	D	a
H_2O, 3 parameter fit	0.634(68)	−2.366	-	11.60(1.62)	1.886(64)
H_2O, 4 parameter fit	0.643(63)	-	−2.655(309)	2.63(45)	1.872(66)
NH_3, 3 parameter fit	0.659(81)	−2.341	-	33.02(7.10)	1.348(93)
NH_3, 4 parameter fit	0.704(83)	-	−3.300(388)	1.09(19)	1.246(93)

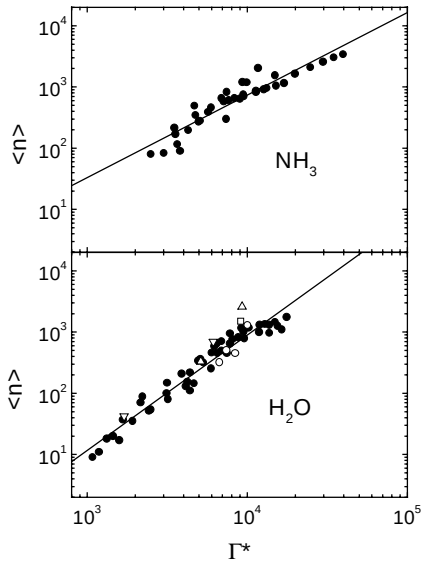

Fig. 4. Average cluster size as function of the reduced scaling parameter for ammonia and water clusters. This work (•); reference [36] (○); reference [35] (△); reference [37] (▽); reference [34] (□).

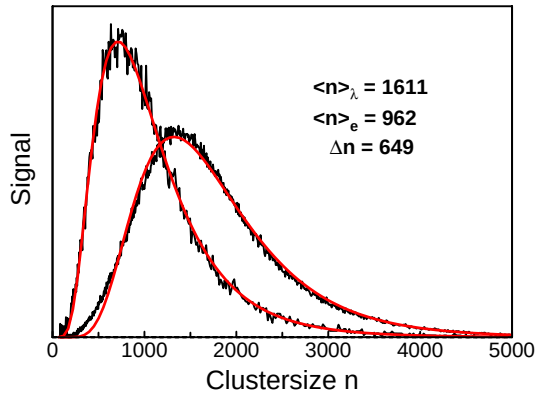

Fig. 5. Measured mass spectra of ammonia clusters obtained under the same source conditions, but detected by photoionization (index λ) and by electron impact at 150 eV (index e). The sizes are determined from the fitted log-normal distributions specified by the solid lines. Δn is the number of evaporated molecules.

out a new fit treating α as additional free parameter instead of assuming $(q-3)$ as exponent of the temperature dependence. For water we got good agreement in q and $q-3$ or α with $q-\alpha=3.3$ instead of 3.0. For ammonia the exponents for the temperature dependence differ with $q-\alpha=4.0$. But we note that the χ^2 value of this fit is only improved by 16% when α is used as free parameter. Therefore we think that equation (2) with $\Gamma = n_0 d^q T_0^{q-3}$ is still a good approximation to describe the size dependence of these two systems.

In general we claim that for the molecular hydrogen bonded systems investigated here, the extended law of Hagena is well reproduced and thus we give reliable parameters for a prediction of the mean clustersize $\langle n\rangle$ from the source conditions. For further comparison we depicted in Figure 4 the reported water cluster sizes of other groups scaled with the parameters obtained here. The results of two electron diffraction measurements [34,35] and two mass spectrometer studies [36,37] follow nicely our data curves. We note that values which correspond to sizes close to the monomer have been omitted in the comparison, since in this size range the measurements are not very reliable and the scaling laws also partly loose their applicability. In reference [37] a similar approach as our 4 parameter fit was tried for water clusters with the result $q=0.63$ and $\alpha=-3.1$ in reasonable agreement with our results.

We conclude that the simple scaling law of Hagena [16] can also be applied to hydrogen bonded molecular systems, if the correct values of the degrees of freedom are used. The reducibility, however, does not work for these systems as can be seen in Figure 4 where the slope and also the absolute values for the two investigated systems are different.

3.2 Fragmentation

Having established a reliable method to measure the size distributions of the molecular clusters we can compare them with the results obtained by the ionization with electron impact under the same experimental conditions. A typical result for ammonia for 150 eV electrons and 193 nm (6.42 eV) photons is shown in Figure 5. Both curves can be fitted by log-normal distributions and give the average cluster sizes of $\langle n\rangle = 1\,611$ and $\langle n\rangle = 962$. Thus 649 molecules evaporate when electron bombardment is used for ionization. In case of the electron impact ionization, the spectra were corrected for a small amount of doubly ionized clusters. For details we refer to the analysis of the water clusters. In order to quantify this behavior, we have measured mass spectra for $(NH_3)_n$ clusters under exactly the same source conditions both for 6.42 eV

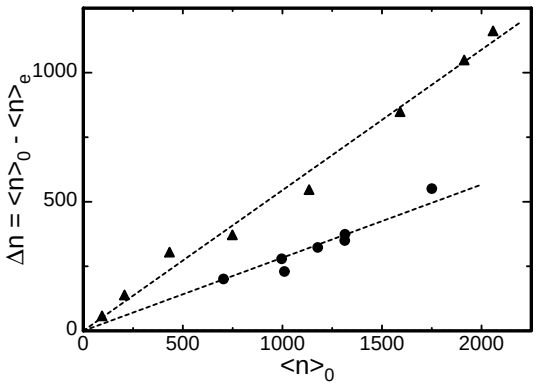

Fig. 6. Number of evaporated molecules as function of the initial cluster size for ammonia (▲) and water (•). The energy of the electron beams is 243 eV for ammonia and 550 eV for water clusters.

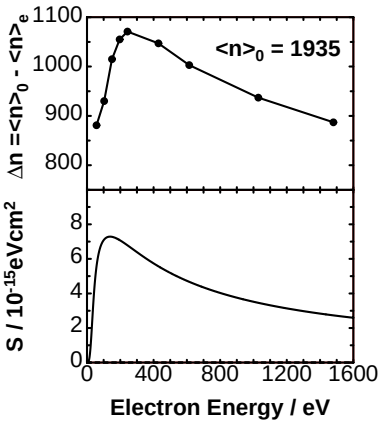

Fig. 7. Upper part: measured energy dependence of the evaporated molecules with electron impact for $(NH_3)_n$ clusters. Lower part: calculated stopping power for the NH_3.

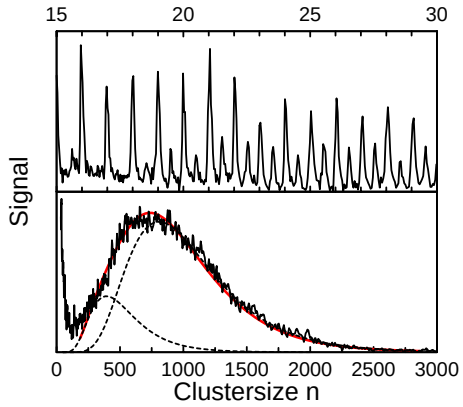

Fig. 8. Upper part: measured mass spectrum of water clusters by electron impact at 550 eV. The doubly charged clusters appear first between $n = 18$ and $n = 19$. Lower part: measured mass spectrum of water clusters by electron impact at 550 eV. The distribution of doubly and singly charged clusters are separately fitted by log-normal distributions.

photons and electrons with the energies 243 eV. For this energy the amount of fragmentation is largest. The result for the size dependence is shown in Figure 6. We define the number of evaporated molecules by

$$\Delta n = \langle n \rangle_0 - \langle n \rangle_\mathrm{e} \tag{7}$$

where $\langle n \rangle_0 = \langle n \rangle_\lambda$ is the average cluster size measured for photons and $\langle n \rangle_\mathrm{e}$ that measured for electrons. Surprisingly, the number of evaporated molecules increases with increasing cluster size and exhibits a nearly linear behavior.

This is in complete contrast of what has been discussed in the introduction about the interaction of *low energy* electrons (20–100 eV) with *small* clusters. In this case the mechanism for fragmentation should decrease with increasing cluster size, since the increasing amount of available degrees of freedom can easier accommodate the energy deposited in the cluster caused by the molecular rearrangement upon ionization.

Apparently, the linear dependence of the number of evaporated molecules from the cluster suggests that the electron interacts in a multiple way with the cluster. The energy release per each event might be constant and independent from the size so that the increase simply results from the increase of events. In order to get more insight into this hypothesis, the dependence of the fragmentation from the electron energy was measured. The result is shown in the upper part of Figure 7 for the average size of $\langle n \rangle = 1\,935$. The energy dependence is quite characteristic. The Δn values first rise to a maximum and then decrease again with increasing electron energy. The maximum occurs at 243 eV.

Very similar results have been obtained for water clusters. The mass spectra measured for electron bombardment exhibit a certain amount of doubly ionized fragments. A typical mass spectrum is depicted in the upper part of Figure 8. Between the mass peaks of the singly ionized water clusters $n = 18$ and $n = 19$ the doubly ionized peaks appear with a threshold at $n = 37$. This is in nice agreement with results obtained previously [38]. Because of the lower mass to charge ratio of the doubly charged products, the size distribution is shifted to smaller values. To correct for this effect, we applied the following procedure. We assume that also the doubly charged clusters follow a log-normal distribution and, instead of fitting one we fitted two log-normal distributions to the experimental data, one of which has the half average value of the other. The result of such a procedure is shown in the lower part of Figure 8. The "true" singly ionized curve is indeed shifted to larger sizes, in the present case to $\langle n \rangle = 963$. The mass spectra obtained by electron impact are corrected in this way.

The mass spectra observed for the ionization by 3.2 eV photons and electrons at 550 eV for two different source conditions are shown in Figure 9. The results of electron impact are corrected for doubly ionized clusters. Again the number of evaporated molecules $\Delta n = \langle n \rangle_0 - \langle n \rangle_\mathrm{e}$ is with 551 and 338 substantial. The dependence from the original cluster size is plotted in Figure 6. As is already observed for ammonia, we find a linear dependence, but the absolute numbers are about a factor of two smaller. The dependence from the electron energy is presented in the upper part of Figure 10 for $\langle n \rangle_0 = 1\,234$. The behavior is again very similar to that observed for ammonia.

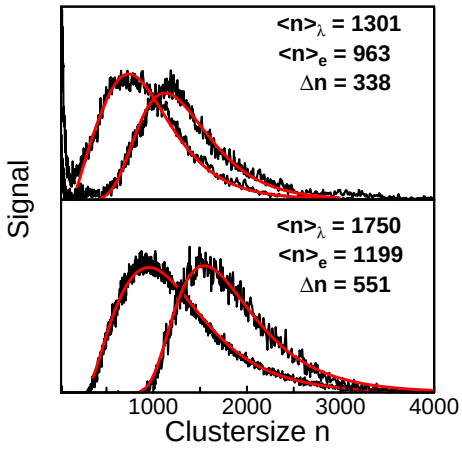

Fig. 9. Measured mass spectra of water clusters obtained under the same source conditions, but detected by photoionization (index λ) and by electron impact at 550 eV (index e). The sizes are determined from the fitted log-normal distributions specified by the solid lines. Δn is the number of evaporated molecules.

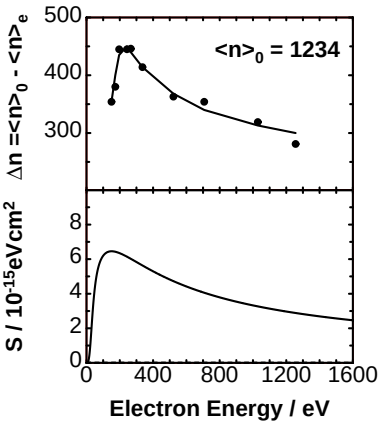

Fig. 10. Upper part: measured energy dependence of the evaporated molecules with electron impact for $(H_2O)_n$ clusters. Lower part: calculated stopping power for the H_2O.

Such a behavior is typical for the energy dependence of the stopping power that charged particles experience when they penetrate into a solid. Thus we would like to compare these results with the stopping cross-section $S = (\mathrm{d}E/\mathrm{d}s)/\rho$, the energy loss per unit path length and density, for electrons in ammonia and water. The usual Bethe formula [39] is only valid in the high energy part of the distribution. On the other hand, direct data in the low energy regime for electrons impinging on the ammonia and water are quite rare. Thus we follow the procedure to convert the well measured data for the proton stopping power [40] to the electron stopping power by looking for data taken at the same velocity [41]. In the article of Greene and Peterson [41] this procedure has been carried out for a series of data sets and we use in what follows their explicit parameterization for ammonia and water given in Table 4 and Figure 6.

The results are shown in the lower parts of Figures 7 and 10, respectively. The agreement of the calculated curves with the measured amount of evaporated molecules is striking. The steep rise, the maximum, and the slower decrease are all reproduced. The positions of the maxima

Table 4. The sputtering yield Y of the condensed phase or the number of ejected molecules Δn of a cluster of the average size $\langle n \rangle$.

	Y or Δn
NH_3, $\langle n \rangle = 1\,935$	881–1 070
NH_3, $\langle n \rangle = 1\,203$	390–593
H_2O, $\langle n \rangle = 1\,234$	281–446
H_2O, condensed	2–20

occur at slightly smaller energies but still within the experimental errors of both curves. This agreement suggests that probably the same mechanisms operate in clusters in the studied energy regime that are operating during the sputtering of these insulator solids under the attack of charged particles.

This is a well studied field with many experimental results and the associated theoretical explanations [13,14]. The sputtering of these weakly bound insulator materials is dominated by electronic interactions and consists of three separate processes. First, the incoming particle interacts with the target and generates electronic excitations and ionizations along the track. Second, these excitation or electron-hole pairs deposit energy into the solid as a result of non-radiative relaxations or repulsive decays which appear as kinetic energy of the molecules. This energy has to be transported to the surface where, finally, the particles evaporate. In the regime of low excitation density, the yield, the number of ejected particles per incoming electron or charged particle, is written as $Y = \Delta z/\lambda_\mathrm{e}$ in which λ_e is the mean spacing between excitations and Δz is the mean depth from which an excitation can lead to ejection weighted over possible ejection processes. A charged particle produces a track of excitations and ionizations along its path through the solid. Here we have $\lambda_\mathrm{e}^{-1} = (\mathrm{d}E/\mathrm{d}s)/W$, where $(\mathrm{d}E/\mathrm{d}s)$ is the electronic stopping power and W the averaged energy deposited in the solid which is effective for the sputtering. Δz is determined by the kinetic energy release to the target ΔE, the cohesive energy of the solid U and a characteristic distance l between the molecules giving $\Delta z = cl\Delta E/U$. The constant c is 0.1–0.2 as was shown in molecular dynamics simulations [42]. The ratio $\Delta E/W$ varies from 0.1 to 0.3. The distance l is either the spacing between two layers or is obtained from the reciprocal of the density and the collision cross-section. Thus the yield is given by

$$Y = c\frac{\Delta E}{W}\left(\frac{\mathrm{d}E}{\mathrm{d}x}\right)\frac{l}{U}\,. \tag{8}$$

In many cases the yield is indeed found to be proportional to the stopping power. This is also valid for molecular targets [43,44]. In some cases, *e.g.* for nitrogen, a transition from the linear to a quadratic behavior is observed [14,44]. This is traced back to a higher excitation density that produces a transiently heated cylindrical region moving to the surface. For ice a pure quadratic dependence is found [14,45] while results for ammonia are not available. The yields are in the range of 1 to 3 in the

linear regime and 10 to 20 in the quadratic part. We note that this sputtering model contains all contributions from electronic excitations and ionization processes with secondary electrons and their conversion into kinetic energy of the lattice in W and ΔE, respectively.

The results for the clusters clearly demonstrate that in case of electron bombardment the yield is always proportional to the stopping power ($\mathrm{d}E/\mathrm{d}s$). Figures 7 and 9 show convincingly the similarity of the results. Here the calculated stopping cross-sections $S = (\mathrm{d}E/\mathrm{d}s)/\rho$ with the density ρ are plotted and compared with the measurement of the number of evaporated molecules Δn that is in the language of the sputtering community equal to the yield Y, the number of ejected particles per incoming projectile. The yield observed for the clusters is given in Table 4 together with the corresponding values for ice [14]. The range of the values is caused by the different initial energy of the projectile.

Thus we conclude that the mechanism which leads to the fragmentation of the clusters is very similar as in electronic sputtering of the corresponding solids. The absolute values of the yield, however, are two orders of magnitude larger than in the case of the solids. Simple geometric considerations of the larger surface area of clusters cannot explain these large differences.

We think that the reason for these discrepancies is the finite dimension of the latter ones. This is explained by a simple model based on the fast distribution of heat after the excitation of a small finite sample. During the penetration of the electrons through the matter the primary electronic excitation and ionization processes lead with the help of electron-phonon coupling to vibrational excitation of the target molecules. The spread of this energy can be described by the heat equation of a temperature field $T(t, r)$ which is a function of the time t and the spatial coordinate r. The solution of the linear heat equation for a point source with the released energy H is [46]

$$T(r,t) = \frac{H}{\rho c_\mathrm{p} (4\pi D t)^{3/2}} \exp\left(-\frac{r^2}{4Dt}\right) \qquad (9)$$

with the density ρ, the specific heat at constant pressure c_p, and the heat diffusivity D which is related to the thermal conductivity λ by $D = \lambda/(\rho c_\mathrm{p})$. It is interesting to note that the same equation is also used for describing the heat distribution in laser ablation [47]. According to equation (9) the spread of the energy distribution is calculated for different times for ice using published material parameters $D = 1.2 \times 10^{-6}$ m^2/s, $c_\mathrm{p} = 2\,040$ J/(kgK), and $\rho = 917$ kg/m^3 [46]. The result is plotted in Figure 11. Already after 15 ps the energy spreads over about 10 nm. This result can also be expressed according to equation (9) by a characteristic heat diffusion length $l_T \approx 2(D\tau)^{1/2}$ where τ is the relaxation time for electron–phonon coupling. With a typical value of $\tau = 20$ ps we obtain $l_T = 10$ nm, in good agreement with the previous result. This spread is, of course, completely irrelevant for a solid of normal dimensions. Our investigated clusters, however, have at best a diameter of 5 nm. Obviously the cluster cannot accommodate the excitation energy and nearly evaporates completely. That is exactly what we observe for the clusters. This also explains why we observe a linear dependence from the stopping power. The quadratic dependence stems mainly from the transportation of the energy to the surface. This is for clusters an irrelevant process. Here the cluster behaves differently in a size range in which other physical and chemical properties adopt already the behavior of the solid.

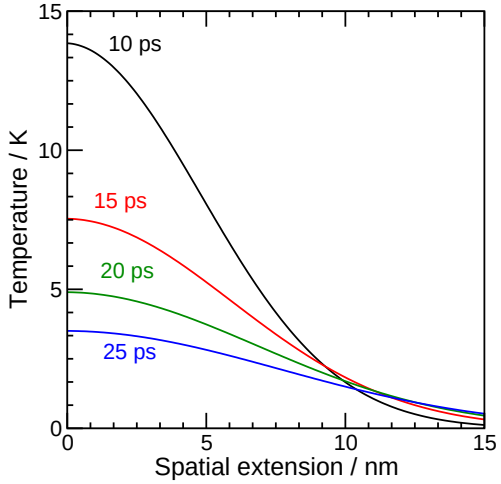

Fig. 11. Calculated spatial distribution of the temperature for the indicated times after the excitation of ice with 400 eV electrons.

If we compare results obtained for the two systems, it is obvious that the number of evaporated molecules (see Fig. 6 and Tab. 4) is, for the same cluster size, larger for ammonia than for water, while the difference in the stopping power is small, see Figures 7 and 10. The reason is probably the larger binding energy of water, 480 meV, compared to 303 meV for ammonia which forces the cluster to evaporate a smaller number of molecules. We note that this evaporation is a very effective process to annihilate the energy of the projectile. In the example presented in Figure 7 an ammonia cluster of $\langle n \rangle = 1\,935$ looses 1 070 molecules after electron impact at 243 eV. Here, nearly all of the energy of the electron beam is used, even if we account for the effect that the binding energy reduces from 303 meV of the solid to 170 meV for small clusters.

The general results found for ammonia and water clusters are in line with the results obtained for the rare gas clusters [12]. These are (i) the increase of the number of evaporated molecules with increasing cluster size, (ii) the pronounced energy dependence which follows exactly that of the stopping power, and (iii) the much higher yield than that observed for the corresponding solids. Apparently, the same mechanism is operating for these weakly bound insulator systems, although the binding energy differs by more than a factor of five.

4 Conclusions

In this contribution we have investigated large ammonia and water clusters in the size range $\langle n \rangle = 10$ to 3 400.

The clusters are detected with nearly no fragmentation by single photon ionization after they have been doped by one sodium atom. For ammonia also a (1+1) resonance enhanced multi-photon ionization (REMPI) scheme has been found *via* the $\tilde{A}$ state in $v = 6$ which serves the same purpose. The measured mass distributions mainly follow log-normal distributions and the resulting average sizes have been analyzed using a modified scaling law in the spirit of that derived by Hagena [16] for rare gases taking into account the different number of degrees of freedom of these molecules.

In contrast, if we use electron bombardment for ionization in the energy range from 150 to 1 500 eV, appreciable fragmentation occurs. From the measured energy dependence, we conclude that the mechanism which is responsible for this fragmentation is the same as that operating for the sputtering of the corresponding solids. The charged particle produces electronic excitations and electron-hole pairs along the track which deposit energy into the vibrational motion of the cluster molecules. Therefore the energy dependence follows the stopping cross-section and the yield of evaporated molecules increases with increasing cluster size. In contrast to the behavior of the solids, the heat spreads fast over the complete cluster which cannot anymore accommodate the energy and strongly evaporates.

This work was supported by the Deutsch Forschungsgemeinschaft. We acknowledge useful discussions with T.D. Märk, J. Schou, and M. Faubel on the sputtering problem.

References

1. See several articles in *Clusters of Atoms and Molecules*, edited by H. Haberland (Springer, Berlin, 1994).
2. T.D. Märk, in *Linking the Gaseous and Condensed Phases of Matter*, edited by L.G. Christopherou *et al.* (Plenum Press, New York, 1994), p. 155, and references cited therein.
3. H. Haberland, Surf. Sci. **156**, 305 (1985).
4. M. Amarouche, G. Durand, J.P. Malrieu, J. Chem. Phys. **88**, 1010 (1988).
5. U. Buck, J. Phys. Chem. **92**, 1023 (1988).
6. U. Buck, H. Meyer, J. Chem. Phys. **84**, 4854 (1986).
7. U. Buck, C. Lauenstein, J. Chem. Phys. **92**, 4250 (1990).
8. U. Buck, M. Winter, Z. Phys. D **31**, 291 (1994).
9. P. Lohbrandt, R. Galonska, H.J. Kim, M. Schmidt, U. Buck, in *Atomic and Molecular Beams*, edited by R. Campargue (Springer, Berlin, 2000), p. 623.
10. R. Karnbach, M. Joppien, J. Stapelfeld, J. Wörmer, T. Möller, Rev. Sci. Instrum. **64**, 2838 (1993).
11. S. Schütte, U. Buck, Appl. Phys. A **69**, S209 (1999).
12. S. Schütte, U. Buck, Intern. J. Mass. Spectrom. (2002, in press).
13. R.E. Johnson, J. Schou, Mat. Fys. Medd. Dan. Vid. Selsk. **43**, 403 (1993).
14. R.E. Johnson, B.U.R. Sundquist, Physics Today, 28 (March 1992).
15. I.V. Hertel, C. Hügin, C. Nitsch, C.P. Schulz, Phys. Rev. Lett. **67**, 1767 (1991).
16. O.F. Hagena, Surf. Sci. **106**, 101 (1981).
17. O.F. Hagena, Z. Phys. D **4**, 291 (1987).
18. D. Proch, T. Trickl, Rev. Sci. Instrum. **60**, 4 (1989).
19. E.R. Rohwer, R.C. Beavis, C. Köster, J. Lindner, J. Grotemeyer, E.W. Schlag, Z. Naturforsch. **43a**, 1151 (1988).
20. S. Schütte, Max-Planck-Institut für Strömungsforschung, Report 7 (1997); Ph.D. thesis, University of Göttingen, 1996.
21. R.N. Barnett, U. Landman, Phys. Rev. Lett. **70**, 1775 (1993).
22. K. Hashimoto, K. Morokuma, J. Am. Chem. Soc. **116**, 11436 (1994).
23. C.J. Mundy, J. Hutter, M. Parrinello, J. Am. Chem. Soc. **122**, 4837 (2000).
24. C. Steinbach, U. Buck, unpublished results.
25. H. Shinohara, N. Nishi, Chem. Phys. Lett. **141**, 292 (1987).
26. E.M. Snyder, J. Purnell, S. Wei, S.A. Buzza, A.W. Castleman Jr, Chem. Phys. **207**, 355 (1996).
27. L.D. Ziegler, J. Chem. Phys. **82**, 664 (1985).
28. K. Fuke, R. Takasu, F. Misaizu, Chem. Phys. Lett. **229**, 597 (1994).
29. K. Fuke, R. Takasu, Bull. Chem. Soc. Jpn. **68**, 3309 (1995).
30. U. Buck, R. Krohne, S. Schütte, J. Chem. Phys. **106**, 109 (1997).
31. J.M. Soler, N. Garcia, O. Echt, K. Sattler, E. Recknagel, Phys. Rev. Lett. **49**, 1857 (1982); C.R. Wang, R.B. Huang, Z.Y. Liu, L.S. Zheng, Chem. Phys. Lett. **227**, 103 (1994).
32. J. Huang, L.S. Bartell, J. Phys. Chem. **99**, 3924 (1995).
33. H. Ashkenas, F.S. Sherman, *Rarefied Gas Dynamics*, edited by J.H. de Leeuw (Academic Press, New York, 1965), Vol. 2, p. 784.
34. G. Torchet, P. Schwartz, J. Farges, M.F. de Feraudy, B. Raoult, J. Chem. Phys. **79**, 6196 (1983).
35. G.D. Stein, J. Armstrong, J. Chem. Phys. **58**, 1999 (1973).
36. M. Ahmed, C.J. Apps, C. Hughes, J.C. Whitehead, J. Phys. Chem. **98**, 12530 (1994).
37. A.A. Vostrikov, D.Y. Dubov, Z. Phys. D **20**, 429 (1991).
38. O. Echt, T.D. Märk, in *Clusters of Atoms and Molecules*, edited by H. Haberland (Springer, Berlin, 1994), Vol. 2, p. 183.
39. L. Reimer, *Scanning Electron Microscopy* (Springer, Berlin, 1984).
40. W. Whaling, *Encyclopedia of Physics* (Springer, Berlin, 1958), Vol. 34, p. 193.
41. A.E.S. Green, L.R. Peterson, J. Geophys. Res., Space Phys. **73**, 233 (1968).
42. S. Cui, R.E. Johnson, P. Cummings, Surf. Sci. **207**, 186 (1988).
43. O. Ellegaard, J. Schou, H. Sørensen, P. Børgesen, Surf. Sci. **167**, 474 (1986).
44. R.E. Johnson, M. Pospieszalka, W.L. Brown, Phys. Rev. B **44**, 7263 (1991).
45. W.L. Brown, W.M. Augustiynik, L.J. Lanzerotti, R.E. Johnson, R. Evatt, Phys. Rev. Lett. **45**, 1632 (1980).
46. U. Grigull, H. Sandner, *Wärmeleitung* (Springer, Berlin, 1979), p. 105.
47. W. Bräuchle, *Thermal, Photophysical, and Photochemical Processes* (Springer, Berlin, 1993), p. 19.